Conf-950683--2

PNL-SA-25626

# EFFECT OF A-SITE CATION DEFICIENCY AND YSZ ADDITIONS ON SINTERING AND PROPERTIES OF DOPED LANTHANUM MANGANITE

J. W. Stevenson
T. R. Armstrong
W. J. Weber

June 1995

Presented at the
Fourth International Symposium on Solid Oxide Fuel Cells Conference
June 18-23, 1995
Yokohama, Japan

Prepared for
the U.S. Department of Energy
under Contract DE-AC06-76RLO 1830

Pacific Northwest Laboratory
Richland, Washington 99352

# EFFECT OF A-SITE CATION DEFICIENCY AND YSZ ADDITIONS ON SINTERING AND PROPERTIES OF DOPED LANTHANUM MANGANITE

J.W. Stevenson, T.R. Armstrong, and W.J. Weber
Materials Sciences Department
Pacific Northwest Laboratory†
Richland, WA 99352

## ABSTRACT

The sintering behavior of Ca- and Sr-doped lanthanum manganite (the preferred SOFC cathode material) is highly dependent on the relative proportion of A and B site cations in the material. In general, A-site cation deficiency increases sintered density. The effect of additions of YSZ to lanthanum manganite (to expand the reactive region at the cathode/electrolyte interface and improve thermal expansion and sintering shrinkage matches) on sintering and other properties will also be reported.

## INTRODUCTION

Lanthanum manganite, $LaMnO_3$, is the preferred material for solid oxide fuel cell (SOFC) cathodes. The severe demands placed upon the cathode during SOFC operation greatly reduce the number of viable candidate materials. The cathode material must be stable in air at 1000°C and have high electronic conductivity. Thermal expansion must be compatible with the yttria-stabilized zirconia (YSZ) electrolyte, and chemical interaction with the electrolyte and interconnect materials must be minimal. Also, the cathode material must maintain a porous microstructure during operation to allow adequate diffusion of gaseous oxygen through the cathode to the cathode/electrolyte interface. When doped with an appropriate amount of Ca or Sr, $LaMnO_3$ offers adequate electrical conductivity, reasonable thermal expansion match to YSZ, and stability in the SOFC cathode operating environment(1-4). Reproducible fabrication of SOFCs requires a thorough knowledge of the sintering behavior of the chosen cathode material. Important factors affecting manganite densification include temperature, type and amount of dopant, and cationic stoichiometry (i.e., relative proportion of A and B site cations).

While SOFC cathodes are typically fabricated using lanthanum manganite (in which electronic conduction predominates), two-phase cathodes consisting of a mixture of an electronic conductor and an ionic conductor (e.g., YSZ) have also been considered(5-10). Advantages over the single-phase cathode may include an expanded oxygen reduction region adjacent to the cathode/electrolyte interface, and improved thermal expansion match

†Operated for the U.S. Dept. of Energy by Battelle Memorial Institute under contract DE-AC06-76RLO 1830.

and sintering shrinkage match between the cathode and the electrolyte. Potential disadvantages of YSZ additions include reduced electrical conductivity and reactions between the manganite and YSZ resulting in the formation of deleterious additional phases. For this study, several manganite compositions were selected based on their close thermal expansion match to YSZ: $(La_{0.84}Sr_{0.16})_xMnO_3$ [LSM-16], $(La_{0.76}Sr_{0.24})_xMnO_3$ [LSM-24], and $(La_{0.80}Ca_{0.20})_xMnO_3$ [LCM-20], with x representing the A/B cation ratio. The effects of YSZ additions (varying from 15 to 60 vol.%) on densification, thermal expansion, and electrical conductivity were examined.

## EXPERIMENTAL PROCEDURE

The required manganite compositions were synthesized using the glycine-nitrate process(11), a combustion synthesis technique which yields high surface area, compositionally homogeneous powders. La, Ca, Sr, and Mn nitrate solutions were mixed in appropriate proportions with glycine. A stoichiometric glycine/nitrate molar ratio was used(12). This mixture was heated until combustion occurred, after which the resulting ash was "pre-calcined" at 650°C for 0.5 hour to remove residual organic material. Subsequent calcinations (with a 1 hour dwell time at the calcination temperature) were performed as needed. YSZ/lanthanum manganite mixtures were produced by spray drying of slurries obtained by wet-milling the required proportions of commercially prepared YSZ (DKKK HSY-8) and manganite powders (calcined 1000°C) in 50/50 vol.% isopropyl alcohol/water with dispersant and binder. The powders were compacted using uniaxial pressure (55 MPa) followed by isostatic pressure (138 MPa). The compacts were sintered in air using a heating rate of 5°C/min and a dwell time (at the sintering temperature) of 1 hour. Sintered densities were determined by the Archimedes method using ethanol. X-ray diffraction analysis was performed using Cu Kα radiation. Sintering shrinkage was measured by heating green compacts in air from room temperature to 1500°C in a dilatometer at a rate of 2°C per minute. Scanning electron microscopy was also performed.

## RESULTS AND DISCUSSION

Doped $LaMnO_3$ has a perovskite-type structure. The sintering behavior of these manganites is highly dependent on the ratio of A-site cations (La, Sr, Ca) to B-site cations (Mn) in the material. LSM-16, LSM-24, and LCM-20 were prepared with A/B cation ratios of 0.91, 0.95, 0.98, 1.00, 1.02, and 1.05. LSM-10 with A/B = 0.98 was also prepared. Since A and B sites are present in a 1:1 ratio, and all ions present in the structure occupy regular lattice sites(13), those ratios would correspond to $(La_{1-y}M_y)_{0.91}MnO_3$, $(La_{1-y}M_y)_{0.95}MnO_3$, $(La_{1-y}M_y)_{0.98}MnO_3$, $(La_{1-y}M_y)MnO_3$, $(La_{1-y}M_y)Mn_{0.98}O_3$, and $(La_{1-y}M_y)Mn_{0.95}O_3$ (M = Ca or Sr), respectively, assuming single phase materials. While compositions near the stoichiometric point (A/B = 1) were single phase perovskites, other compositions contained small amounts of additional phases, as discussed below. Although manganites can also exhibit oxygen nonstoichiometry, that nonstoichiometry in highly doped manganites tends to be relatively small(14). For convenience, therefore, an oxygen stoichiometry of 3 (rather than $3 \pm \delta$) is used in this article.

Sintered (1350°C for 1 hour) densities for LSM-16, LSM-24 and LCM-20 (calcined at 650°C for 0.5 hour) are shown as a function of A/B cation ratio in Figure 1. The green

densities were essentially independent of A/B cation ratio, whereas the sintered densities were highly dependent on the A/B ratio, with A-cation deficient compositions (A/B ratio < 1) exhibiting substantially higher densities than the stoichiometric and B-cation deficient manganites. This pronounced effect of A/B cation ratio on densification behavior was also observed in measurements of the linear shrinkage of green compacts as a function of temperature. For example, sintering shrinkage plots for LSM-24 are shown in Figure 2. These plots show an enhancement of shrinkage for the A cation deficient manganites. The shape of these shrinkage plots is consistent with a solid state sintering mechanism, with no signs of sudden shrinkage events (nearly vertical regions in the plot) resulting from liquid phase formation.

The higher densities obtained in the A-site cation deficient manganites suggests that the diffusion of A-site cations is the limiting factor in mass transport during densification (15). Preparation of manganites with A/B < 1.00 should result in an excess concentration of A-site vacancies within the structure. When additional A-site vacancies are present in the structure, A-site cation diffusion occurs more readily, allowing for higher sintered densities. This agrees with conclusions drawn by van Roosmalen et al.(16) for undoped lanthanum manganite. Since sintered density was not significantly affected by B-site cation deficiency, the diffusion of B-site cations does not appear to be a limiting factor during sintering.

XRD analysis on crushed specimens after sintering at 1450° C revealed small quantities of additional phases in some compositions. $La_2O_3$ was present in some of the compositions with an A/B ratio greater than 1.00. The presence of $La_2O_3$ in lanthanum manganite materials is undesirable, since $La_2O_3$ tends to absorb atmospheric moisture to form $La(OH)_3$. This hydration process can drastically reduce the strength of the sintered material. $Mn_3O_4$ was observed in compositions with substantial A cation deficiency. In order to avoid formation of $La_2O_3$, the manganites used in the YSZ/manganite mixtures in this study were synthesized with an A/B ratio less than 1.

Sintered densities of LSM-16 and LCM-20 with A/B = 0.98 (calcined at 1000°C for 1 hour) are shown as a function of sintering temperature (with 1 hour sintering time) in Figure 3. In that figure, the plots labeled SD refer to data for powders which were spray dried before compaction, while NSD refers to data for powders which were not spray dried before compaction. Sintered densities increased uniformly with increasing temperature (from 1250 to 1450°C) for LSM-16, with the spray dried powder yielding substantially higher densities than the non-spray dried powder. In the case of LCM-20, densities exhibited a maximum at an intermediate temperature (1400°C for NSD, 1350 for SD). The sintered densities for the spray dried LCM-20 decreased steeply at temperatures above 1350°C. A possible explanation for this behavior is discussed below.

Sintered densities of mixtures of YSZ/LSM-16 and YSZ/LCM-20 are shown in Figures 4 and 5, respectively. Sintered densities for YSZ alone (also shown in Figure 5) increased uniformly with increasing sintering temperature. For the manganite/YSZ mixtures, however, densities increased with increasing temperature until reaching a maximum around 1300°C. At higher temperatures, the densities tended to decrease substantially with increasing temperature. As noted above (see Figure 3), a similar trend was observed in sintered LCM-20, but not in LSM-16. High porosity is essential for the SOFC cathode. It is clear from Figures 4 and 5 that the degree of porosity of the sintered mixtures can be varied over a wide range by changing the sintering temperature. In practice, the introduction of pore formers, such as organic materials which can be removed

at low temperatures, may be a preferable means of obtaining the desired level (and morphology) of porosity.

One of the potential advantages of the addition of YSZ to lanthanum manganite is an improved thermal expansion match between the cathode and the YSZ. Thermal expansion plots for LSM-16, LSM-24, LCM-20 (all with A/B = 0.98), YSZ, and LCM-20 with 15 and 50% YSZ additions (sintered 1300°C) are shown in Figure 6. The average TECs (between 25 and 1000°C) of LSM-16 ($10.0 \times 10^{-6}$ $K^{-1}$) and LCM-20 ($10.5 \times 10^{-6}$) were close to that of YSZ ($10.2 \times 10^{-6}$), but the plots deviated significantly from YSZ at intermediate temperatures. The average TEC for LSM-24 was considerably higher ($11.2 \times 10^{-6}$). These observed values for Sr-doped lanthanum manganite are similar to those reported by Aizawa et al (17) and somewhat lower than values reported by Srilomsak et al (4). For LCM-20, the deviation from YSZ could be eliminated by adding 15% or 50% YSZ. For LSM-16, the addition of 50% YSZ also resulted in a close match to YSZ. However, a 15% addition of YSZ to LSM-16 did not improve the match to YSZ but instead resulted in an increased thermal expansion ($11.1 \times 10^{-6}$).

Some SOFC designs require co-sintering of the cathode and YSZ. Successful co-sintering requires a close match in the sintering behavior of both materials. Plots of sintering shrinkage (with and without YSZ additions) as a function of temperature are shown for LSM-16 and LCM-20 in Figures 7 and 8, respectively. The mismatch between the shrinkages of YSZ and the manganites without YSZ additions is apparent. In the case of LSM-16, the addition of 15 vol.% YSZ improved the match to YSZ significantly, except at high temperature (above 1400°C) where there was evidence of swelling of the specimen. Increasing the addition to 50 vol.% had little further effect on the shrinkage behavior. For LCM-20, the match was improved slightly by the YSZ additions. At high temperatures, substantial swelling was observed in the YSZ/LCM specimens; swelling also occurred to a lesser degree in the YSM/LSM specimens. This swelling may occur as a result of oxygen evolution from the perovskite lattice at elevated temperatures. If the specimen has sintered sufficiently to close off the internal pores from the surface, oxygen leaving the lattice will be trapped within the bulk of the specimen and may cause bloating. This mechanism may explain the low densities observed for the YSZ/manganite mixtures sintered at high temperatures (Figures 4 and 5) as well as the sintering behavior observed for LCM-20 in Figure 3. Regarding Figure 3, at lower and intermediate sintering temperatures, the SD powders achieved higher densities than the NSD powders, suggesting that improved initial powder packing enhanced the densification process. At higher sintering temperatures, however, (at which substantial oxygen evolution may occur) the enhanced sintering may have rapidly sealed off the pores in the specimens, so that bloating due to the subsequent evolution of lattice oxygen resulted in low sintered densities.

Arrhenius plots of the electrical conductivity of LSM-16 and LCM-20 (with and without YSZ additions) are shown in Figures 9 and 10, respectively. The conductivity of YSZ is also shown. As expected, the conductivity of the mixtures decreased with increasing YSZ content. The fact that the activation energies of the manganites (approx. 0.13 eV) were changed only slightly by the YSZ additions is not surprising. Increased YSZ content may substantially increase the ionic conduction within the materials, but (since the electrical conductivity of YSZ is several orders of magnitude lower than that of lanthanum manganite) the bulk conduction is still dominated by the primarily electronic conduction of the manganites.

Lanthanum manganite and YSZ have been observed to form undesirable electrically insulating reaction products (e.g., $La_2Zr_2O_7$ and $Sr_2ZrO_4$ (18,19,20)), at elevated temperatures. In this study, XRD analysis of pulverized sintered (1400°C, 1 hour) specimens of manganite/YSZ mixtures revealed the presence of small quantities of $La_2Zr_2O_7$. For example, YSZ/LSM-10 mixtures contained approx. 5 wt.% $La_2Zr_2O_7$. Similarly, Richards and Singhal (8) reported $La_2Zr_2O_7$ formation when synthesizing LSM-10 with 10 wt.% zirconia by heat-treating oxides and carbonates. In the present study (using LSM-10, 16, and 24), the amount of $La_2Zr_2O_7$ formed was found to decrease with increasing Sr content. In fact, no $La_2Zr_2O_7$ was observed in LSM-24 with 40 and 50 vol.% YSZ additions; only a trace of $La_2Zr_2O_7$ was observed when the YSZ content was 60 vol.%. A small quantity (approx. 1 wt.%) of $La_2Zr_2O_7$ was observed in the LCM-20/YSZ mixtures.

The formation of $La_2Zr_2O_7$ is likely to be a result of the diffusion of Mn cations from the manganite into the YSZ. Mn depletion of the manganite would liberate La to react with the YSZ to form $La_2Zr_2O_7$. This mechanism can be depicted (in Kroger-Vink notation(21)):

$$LaMnO_3 \rightarrow (1-x)\,LaMnO_3 + \frac{x}{2}La_2O_3 + x\,Mn'_{Zr} + \frac{3x}{2}O_O + \frac{x}{2}V_O^{\bullet\bullet} \qquad [1]$$

$$La_2O_3 + 2\,ZrO_2 \rightarrow La_2Zr_2O_7 \qquad [2]$$

This suggests that the use of a "Mn-enhanced" (i.e., substantially A-site cation deficient) lanthanum manganite would be a means of avoiding the formation of $La_2Zr_2O_7$. The presence of surplus Mn would allow for Mn diffusion into the YSZ without causing the manganite to become Mn-depleted.

To test this concept experimentally, highly A-site cation deficient LSM-16 and LCM-20 (A/B = 0.91) were prepared and sintered. XRD analysis of pulverized sintered specimens indicated the presence of approx. 1 wt.% $Mn_3O_4$ as a second phase. Mixtures of those manganites with YSZ (50 vol.% of each) were also prepared and sintered (1400°C). XRD analysis of those specimens revealed no trace of $Mn_3O_4$ or $La_2Zr_2O_7$. The disappearance of the $Mn_3O_4$ and suppression of the formation of $La_2Zr_2O_7$ is consistent with the above mechanism. This suggests that the use of Mn-enhanced lanthanum manganite may eliminate the formation of $La_2Zr_2O_7$ during SOFC fabrication and operation. The electrical conductivities of mixtures utilizing the Mn-enhanced manganites were very similar to the corresponding mixtures using the nearly-stoichiometric (A/B = 0.98) manganites.

## CONCLUSIONS

The sintering behavior of doped lanthanum manganite and yttrium manganite was determined to be highly sensitive to changes in the A/B cation ratio. Manganites synthesized with a deficiency of A-site cations exhibited enhanced densification behavior

relative to B-site cation deficient manganites. Maximum sintered densities of mixtures of lanthanum manganite and YSZ were obtained by sintering at 1300°C. Higher sintering temperatures resulted in lower densities. The addition of YSZ to the manganites resulted in reduced electrical conductivity but allowed for tailoring of the thermal expansion and sintering shrinkage. Small quantities of $La_2Zr_2O_7$ were formed during sintering of mixtures of YSZ and slightly A cation deficient manganites (i.e., A/B = 0.98). The formation of $La_2Zr_2O_7$ during sintering was suppressed in mixtures of YSZ and Mn-enriched manganites (A/B = 0.91). Thus, judicious selection of the A/B cation ratio and amount of YSZ addition may result in SOFC cathodes with adequate electrical conductivity, thermal expansion and sintering shrinkage matched to the YSZ electrolyte, and minimal deleterious interaction with the YSZ.

## ACKNOWLEDGMENTS

The authors thank George Hsieh, Steve Vahey, Brett Lembke, Matt Laine, Ron Stephens, David McCready, and Jim Coleman for their assistance with this work.

## REFERENCES

1. N.Q. Minh, J. Am. Ceram. Soc., **76**, 563 (1993).
2. J.H. Kuo, H.U. Anderson, and D.M. Sparlin, J. Solid State Chem., **83**, 52 (1989).
3. J.H. Kuo, H.U. Anderson, and D.M. Sparlin, J. Solid State Chem., **87**, 55 (1990).
4. S. Srilomsak, D.P. Schilling, and H.U. Anderson, in 1st Intl. Symp. on SOFC/1989, S.C. Singhal, Editor, **PV** 89-11, p.129, The Electrochemical Society Proceedings Series, Pennington, NJ (1989).
5. J. Mizusaki, H. Tagawa, K. Tsuneyoshi, A. Sawata, M. Katou, and K. Hirano, Denki Kagaku, **58**, 520 (1990).
6. T. Kenjo, S. Osawa, and K. Fujikawa, J. Electrochem. Soc., 138, 349 (1991).
7. T. Kenjo and M. Nishiya, Solid State Ionics, **57**, 295 (1992).
8. V. Richards and S. Singhal, J. Mat. Sci. Lett., **11**, 1193 (1992).
9. A. Shiratori, M. Iha, O. Chikagawa, H. Takagi, K. Tomono, and K. Akagi, Fuel Cell Seminar Abstracts, p. 37, Courtesy Associates, Inc. (1994).
10. S. Taniguchi, M. Kadowaki, H. Kawamura, T. Yasuo, Y. Akiyama, Y. Miyake, T. Saitoh, and M Harada, Fuel Cell Seminar Abstracts, p. 41, Courtesy Associates, Inc. (1994).
11. L.A. Chick, L.R. Pederson, G.D. Maupin, J.L. Bates, L.E. Thomas, and G.J. Exarhos, Materials Letters, **10**, 6 (1990).
12. L.A. Chick, G.D. Maupin, G.L.Graff, L.R. Pederson, D.E. McCready and J.L. Bates, Mat. Res. Soc. Symp. Proc., **249**, 159-164 (1992).
13. B.C. Tofield and W.R. Scott, J. Solid State Chem., **10**, 183 (1974).
14. J.W. Stevenson, M.M. Nasrallah, H.U. Anderson, and D.M. Sparlin, J. Solid State Chem., **102**, 175 (1993).
15. J.W. Stevenson, P.F. Hallman, T.R. Armstrong, and L.A. Chick, Accepted J. Am. Ceram. Soc.
16. J.A.M. van Roosmalen, E.H.P Cordfunke, and J.P.P. Huijsmans, Solid State Ionics, **66**, 285 (1993).

17. M. Aizawa, H. Nishiyama, A. Ueno, M. Kuroishi, S. Yoshino, K. Eguchi, and H. Arai, Proc. 36th Int. SAMPE Symp., p. 1231 (1991).
18. O. Yamamoto, Y. Takeda, R. Kanno, and M. Noda, Solid State Ionics, **22**, 241 (1987).
19. O. Yamamoto, Y. Takeda, R. Kanno, and T. Kojima, in 1st Intl. Symp. on SOFC/1989, S.C. Singhal, Editor, **PV** 89-11, p.242, The Electrochemical Society Proceedings Series, Pennington, NJ (1989).
20. O. Yamamoto, Y. Takeda, N. Imanishi, and Y. Sakaki, in 3rd Intl. Symp. on SOFC/1993, S.C. Singhal and H. Iwahara, Editors, **PV** 93-4, p.205, The Electrochemical Society Proceedings Series, Pennington, NJ (1993).
21. F.A. Kroger, The Chemistry of Imperfect Crystals, North-Holland, Amsterdam (1964).

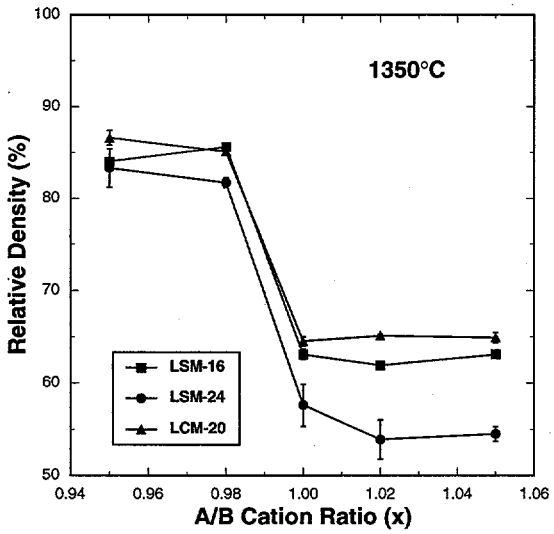


Figure 1. Relative densities of lanthanum manganites as a function of A/B ratio. Specimens sintered in air at 1350°C for 1 hour.

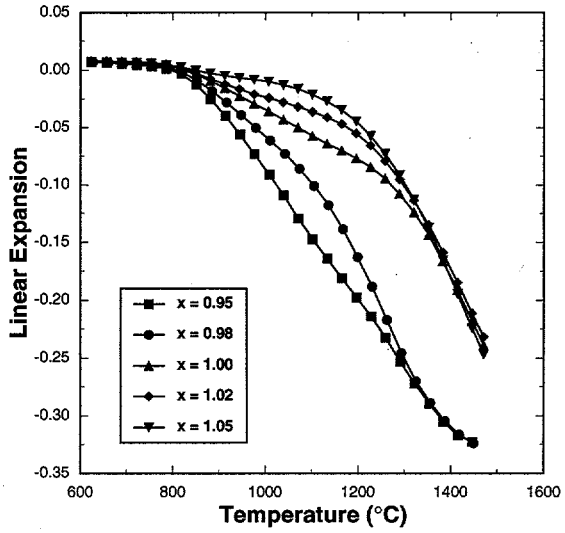


Figure 2. Sintering shrinkage plots for LSM-24 with varying A/B ratio. Specimens heated at 2°C/min in air.

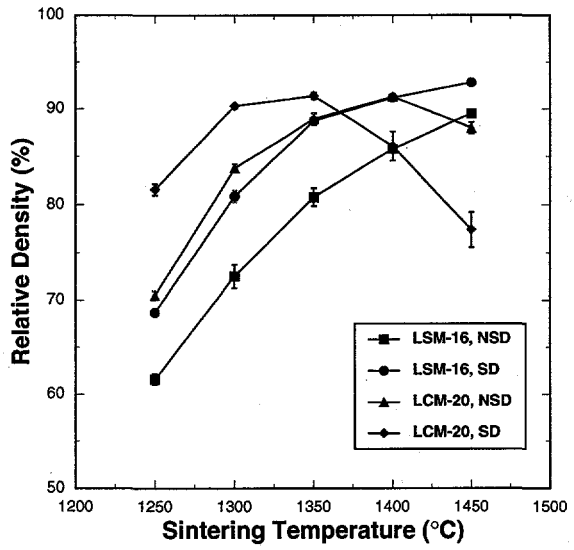


Figure 3. Relative densities of spray dried (SD) and non-spray dried (NSD) lanthanum manganites sintered in air.

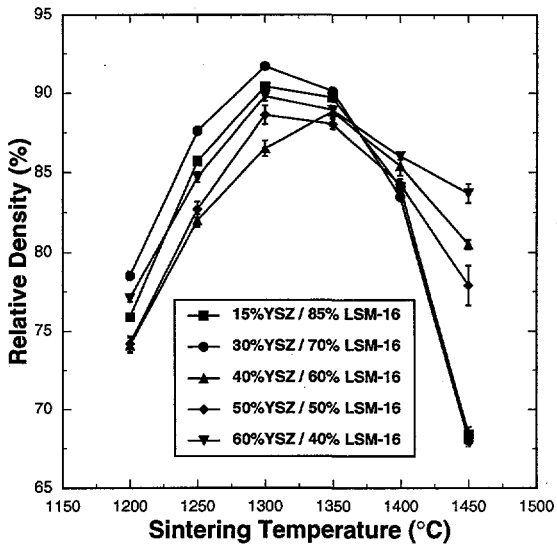


Figure 4. Relative densities of LSM-16/ YSZ mixtures sintered in air at the indicated temperatures.

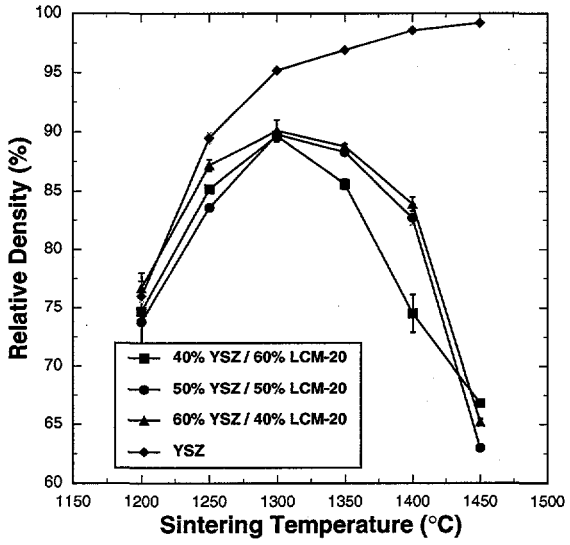


Figure 5. Relative densities of LCM-20/ YSZ mixtures sintered in air at the indicated temperatures.

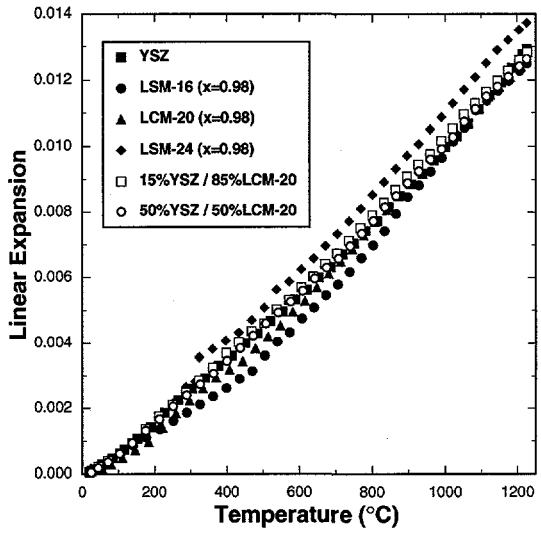


Figure 6. Thermal expansion plots for the indicated compositions. Specimens heated at 2°C/min in air.

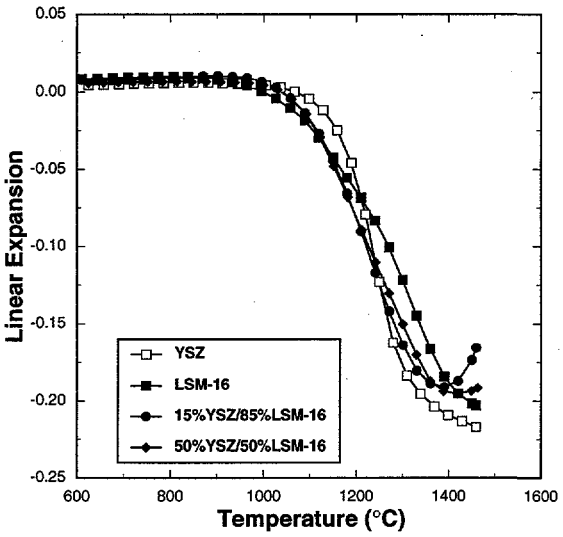


Figure 7. Sintering shrinkage plots for LSM-16/YSZ mixtures. Specimens heated at 2°C/min in air.

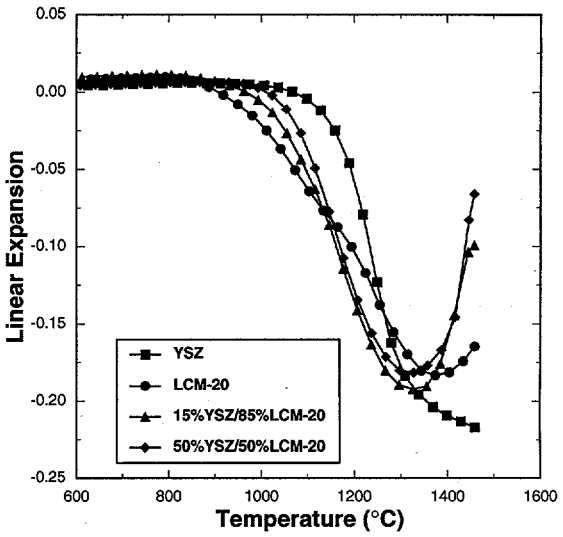


Figure 8. Sintering shrinkage plots for LCM-20/YSZ mixtures. Specimens heated at 2°C/min in air.

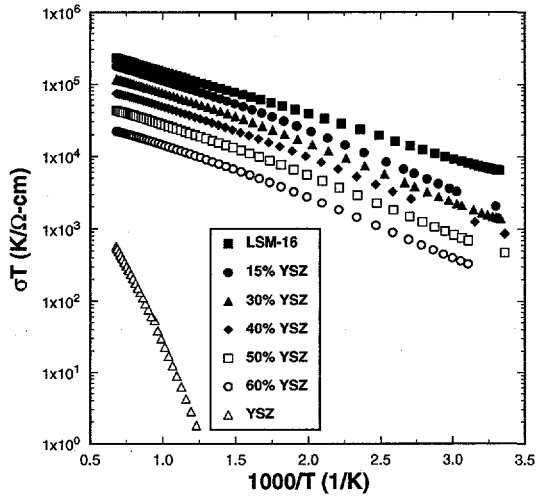


Figure 9. 4-point d.c. conductivity of sintered LSM-16/YSZ mixtures (measured in air).

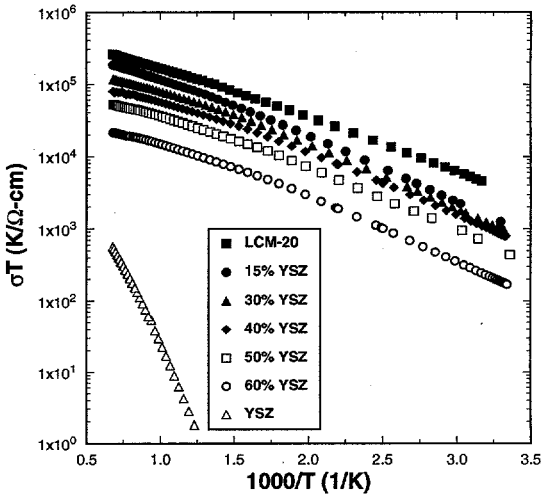


Figure 10. 4-point d.c. conductivity of sintered LCM-20/YSZ mixtures (measured in air).